Proceedings of the Institution of Mechanical Engineers, Part B: Journal of Engineering Manufacture

http://pib.sagepub.com/

Role of Fixture Forces on Distortion in Gas Tungsten Arc Welding — An Experimental and Modelling Approach

F Sikström, A-K Christiansson and B Lennartson

Proceedings of the Institution of Mechanical Engineers, Part B: Journal of Engineering Manufacture 2011 225: 140
DOI: 10.1177/09544054JEM2048

The online version of this article can be found at:
http://pib.sagepub.com/content/225/1/140

Published by:
SAGE
http://www.sagepublications.com

On behalf of:
Institution of Mechanical Engineers

Role of fixture forces on distortion in gas tungsten arc welding – an experimental and modelling approach

F Sikström[1]*, A-K Christiansson[1], and **B Lennartson[1,2]**
[1]Department of Engineering Science, University West, Trollhättan, Sweden
[2]Department of Signals and Systems, Chalmers University of Technology, Gothenburgh, Sweden

The manuscript was received on 27 February 2010 and was accepted after revision for publication on 2 August 2010.

DOI: 10.1177/09544054JEM2048

Abstract: Simulation and experiments show that the fixture clamping force has a significant influence on the structural integrity of a welded workpiece. This understanding is of great importance for the manufacture of aerospace components with tight tolerances in the specifications. The focus in the present study is on the temperature history during welding and residual deformation; its main contribution is a demonstrator designed for evaluation of the influence of fixture clamping forces and validation of the simulation results. The demonstrator concerns a simplified situation considering gas tungsten arc welding of a nickel-based metal plate fixed by a specially designed fixture, where one side of the plate was clamped with different levels of force. The temperature history was measured during the weld sequence and deformation measurements were performed after cooling and release of the workpiece from the fixture. The results from simulation and experimentation showed good agreement. The proposed strategy is industrially competitive and has shown that the looser the fixture clamps, the smaller the residual deformation. Furthermore, the study provides a knowledge base for selection of active fixture concepts in that the fixture clamping force can be determined in advance and possibly also be subject to force control.

Keywords: finite element analysis, gas tungsten arc welding, nickel-based steel, fixture clamping force, residual deformation

1 INTRODUCTION

Welding is being used more and more in aerospace manufacturing, especially for the fabrication of engine parts, where smaller components are joined together to build up vital structures. Weld simulation is being performed to a greater extent with the goals, for example, to predict deformations and to select weld sequences, especially for complicated geometries [**1**]. These simulations are computationally heavy, and normally the weld fixture is included as constant boundary conditions. However, the weld fixture affects the final results considerably, and it would be favourable to take this into consideration at the same time as the weld simulation. This paper presents a demonstrator with the objective to evaluate the influence of fixture clamping forces on residual deformations and to validate simulation results by experimental data. There are numerous examples in the literature of how weld simulations are utilized for predictions of the process influence on structural integrity and how it influences different aspects of mechanical properties. Several examples deal with the question of how to mitigate residual stress and deformation (see e.g. references [**2**] to [**7**]); whereas other examples focus on the physics of heat generation and its influence on mechanical properties (see e.g. references [**8**] to [**11**]). The present work highlights the fact that simulations can be used to predict the fixture's influence on the residual deformation. The focus is on the temperature history and residual deformation, and on calibration of the simulation model.

One project aim is to evaluate and clarify the influence of weld fixtures on the process. It has been shown that the fixture clamping force has a considerable influence on the residual deformation of

**Corresponding author: Department of Engineering Science, University West, Trollhättan, SE 46186, Sweden.*
email: fredrik.sikstrom@hv.se

the part. The other aim is to evaluate simulations where a fixture with variable clamping force is integrated in the weld simulation in order to efficiently be able to predict workpiece distortion as a function of clamping force. A simplified test case has been identified to provide first answers on how well this integrated simulation predicts the residual deformation. Robotized gas tungsten arc welding (GTAW) is performed as bead-on-plate on rectangular nickel-based metal plates. The simple test case is chosen to eliminate the dependency of varying joint quality if a joining was to be performed and to ensure a repeatable motion of the weld torch. The metal plate is clamped stiffly at one side and fixed with varying clamping force on the opposite side. Experiments and simulations are performed with three different clamping forces: stiff, medium, and loose. Simulations have been the basis for selecting these forces. The plate will slide in the fixture when not really stiffly fastened, and to have realistic friction data in the simulation, a specialized fixture was designed for use with a tensile test machine for this estimation. Nominal weld parameters were decided for the chosen material, and the frictional coefficient was measured for the three test cases (stiff, medium, and loose).

It is obvious that the temperature is an important factor for the result, which is why some of the plates were instrumented with thermocouples on strategic places. Residual deformation was simulated using the simulation model and measured using an optical three-dimensional (3D) scanning system. These matters are described in the following in more detail.

2 DEMONSTRATOR SETUP

The demonstrator was built in University West, Sweden, weld laboratory, with robotized GTAW equipment and different measuring systems, described further below. Emphasis was on a realistic but simple enough situation in order to eliminate the influence of irrelevant error sources.

The workpieces used in the demonstrator were superalloy Inconel 718 plates. This alloy is a high-strength, corrosion-resistant nickel–chromium material commonly used in the aerospace industry. The plates were water-cut with outer dimensions 100 mm × 150 mm × 3.17 mm and with five fastening holes along one side. Figure 1 shows one plate and the location of four thermocouples mounted down the weld path. The chemical composition of Inconel 718 is provided elsewhere [**12**].

A fixture was designed to facilitate the variation of clamping forces. Figure 2 shows an exploded view of the final weld fixture design. The metal plate, numbered 1, is the actual workpiece; part 2, with screw holes, maintains the stiff fastening at one side; the cylinder (3) maintains the variable fixture force through the block (4), the yoke (5), and base support (6); the replaceable plates (7a, 7b) ensure the friction to be the same for all welding. The support has a channel for shielding gas. A hydraulic cylinder together with an Enerpac hand pump was used to generate the variable fixture force. The cylinder has an effective area of 4210 mm^2 and a capacity of 295 kN. The cylinder was pumped manually; however, it can be controlled in the future for force feedback control. Figure 3 shows the equipment used for applying the variable clamping force.

2.1 Friction tests

A special fixture was designed for the friction tests. The plates were mounted in the fixture and attached to the tensile test machine, see Fig. 4. The fixture consists of several parts; one is fixed to the moving part of the tensile machine and one to the fixed part. The plate is stiffly fastened with five screws in the fixture to the moving part of the tensile machine (upper part in Fig. 4). The other part of the plate is resting freely in the fixture part that is fastened in the stiff grip of the tensile machine. The remaining parts

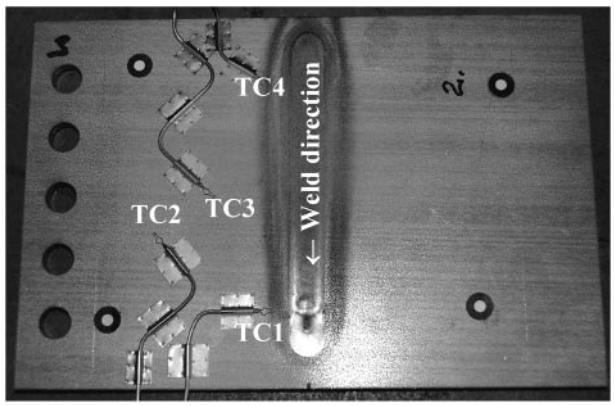

Fig. 1 Plate instrumented with thermocouples (TC1–TC4) after welding

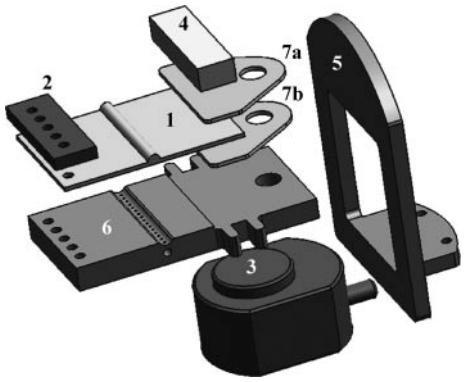

Fig. 2 Exploded view of the weld fixture

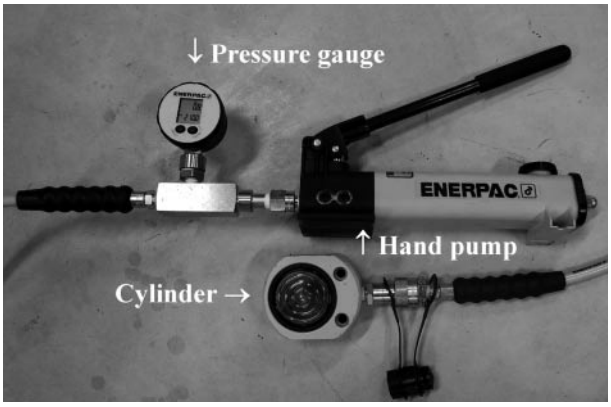

Fig. 3 Components used for varying the fixture force

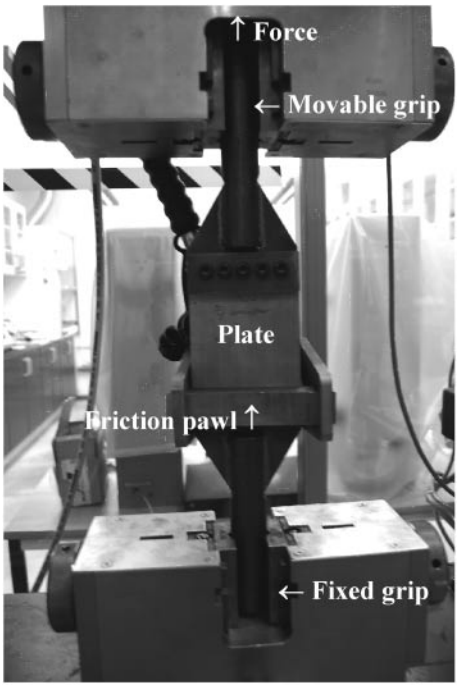

Fig. 4 Friction test in the tensile test machine

of the fixture are used to clamp the freely resting part of the plate with different clamping forces using the same equipment as for the weld fixture. The tensile test machine applied an increasing force, and at a certain value the plate started to slip in the fixture. The smoother were the plates, the more reproducible was the result. For this reason the weld trials were performed with the same roughness of the supporting fixture parts. In total 55 tests were performed to form a statistical average of the frictional coefficient and to evaluate the consequences of wearing of the sliding surfaces.

2.2 Weld experiment

Autogenous bead-on-plate welding was carried out in an in-house robotized welding cell on six plates. The

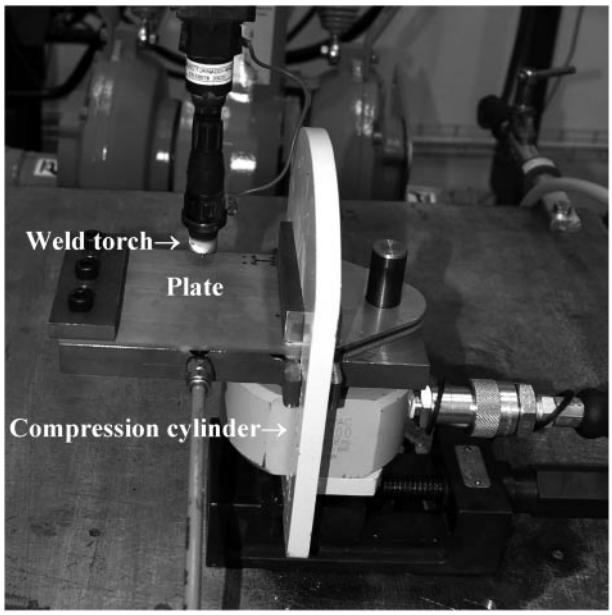

Fig. 5 Setup in the welding cell

weld arc was ignited and, after a preheating time of 2 s, the weld motions started with a velocity of 2 mm/s. The welds started 10 mm from the edge of the plate and stopped 10 mm from the opposite edge. The power source used was a TIG Commander 400 AC/DC from Migatronic AB, and the weld torch was a Binzel Tornado WH0 from Alexander Binzel Schweisstechnik GmbH & Co. A thoriated tungsten electrode WT20 from Wolfram Industrie GmbH and argon as shielding gas were used. The weld torch was mounted on the tool centre-point of an IRB 1400 industrial robot from ABB Robotics in order to attain precise motions with satisfactory repeatability. Figure 5 shows the setup in the welding cell, Table 1 provides the nominal weld parameters used.

2.3 Measurements

The plates were instrumented with thermocouples, type K, according to Fig. 1 in order to acquire the temperature history of interest. All measured data were recorded and stored in a file for post analysis. A measurement module from National Instruments Corporation was used for thermocouple data acquisition, and the signal processing was implemented in National Instrument's LabVIEW software.

To validate the mechanical simulation the residual deformation was measured using a commercial 3D scanner called ATOS III, a structured light system developed by GOM GmbH (see e.g. reference [**13**]). Two cameras and a fringe pattern projector were mounted on a tripod in front of the workpiece. Fringe patterns were projected onto the workpiece and were observed by two charge-coupled device (CCD) cameras. The plate surface was 3D-scanned loose

Table 1 Nominal weld and fixture parameters

Parameter	Value	Unit
Electrode diameter	2.4	mm
Electrode tip angle	45	degrees
Arc length	1.7	mm
Work angle	0	degree
Weld travel speed	2	mm/s
Shielding gas flow	16	l/min
Weld current, I	120	A
Arc voltage, V	17	V
Arc efficiency, η	0.75	–
Forces, stiff/medium/loose	295/84/0	N

(before being clamped in the fixture), when clamped before and after welding, and finally after cooling and release: in total four scans of each plate. The deviations between the measurements before and after weld were calculated, thus giving a measure of the deformations caused by the weld process.

3 WELD MODELLING

The modelling of heat transfer in a welded workpiece involves a number of physical phenomena such as the arc–metal interaction, fluid flow in the weld pool, non-linear heat transfer in the workpiece, and the associated boundary conditions. The modelling here is limited to transient heat conduction, which means that geometrical boundaries are fixed with no surface deformations in the top or root surface and with no fluid flow in the weld pool. Since the model is not capable of predicting how molten metal flows within the weld pool, it exhibits systematic errors. The explanation is that convection dominates heat transfer in the weld pool (see e.g. reference [**11**]). Still, this approximation is used by many authors due to its ability to give reasonably accurate predictions (see e.g. references [**14**] to [**17**]). The heat input from the weld arc is modelled by a volumetric, Gaussian distribution-shaped [**4**] heat flow density in which some of the physics is simplified and aggregated in a few parameters. The thermal boundary conditions are defined by coefficients that are assumed to be constant.

In the structural analysis the workpiece has been modelled as a homogeneous, isotropic, elastoplastic material exhibiting rate-independent, isotropic hardening with a von Mises yield surface and the associated flow rule. Strains and displacements are assumed to be large, and it is assumed that no creep strains occur during welding as the material is exposed to a high temperature for a very short period of time. Transformation plasticity is not accounted for in the model. The classical theory of elasticity and thermo-plasticity is used [**5**]. Friction is a complex physical phenomenon that involves the characteristics of the surface such as surface roughness, temperature, normal stress, and relative velocity. The modelling of friction has been simplified to the commonly used Coulomb friction model [**18**].

3.1 Thermal model

To predict the temperature field in the workpiece during welding, transient heat transfer has been modelled by a non-linear heat conduction equation with temperature-dependent coefficients.

The partial differential equation is defined in a Lagrangian reference frame [**5**]

$$\rho C_{\text{eff}} \frac{\partial T}{\partial t} + \nabla(-k\nabla T) = Q \tag{1}$$

where T denotes temperature. The coefficients are density $\rho(T)$, effective heat capacity $C_{\text{eff}}(T)$, and heat conductivity $k(T)$. The term Q models the heat source. The initial temperature is assumed to be homogeneous room temperature of 300 K.

Boundary conditions define how heat is transferred from the workpiece to its ambient atmosphere. Natural boundary conditions are commonly described as [**5**]

$$k\frac{\partial T}{\partial n} + h_{\text{c}}(T - T_{\text{amb}}) + \varepsilon\sigma(T^4 - T_{\text{amb}}^4) = 0 \tag{2}$$

The coefficient k in the conduction term is the same heat conductivity coefficient as in equation (1), and $\partial T/\partial n$ is the normal derivative, i.e. the derivative in the outward normal direction to the workpiece surface. The convection term is defined by the material-dependent convection heat transfer coefficient h_{c}. The radiation term is defined by the product of a temperature-independent total hemispherical emissivity ε and the Stefan-Boltzmann constant σ ($=5.67040\times10^{-8}$ W/m^{2}K^4). T_{amb} is the ambient temperature that is assumed to be close to room temperature. Generally there are separate sections of a workpiece surface where different terms in equation (2) are dominating. Some sections are in contact with the fixture and assumed to be governed by pure conduction, since a workpiece typically is clamped with a large force. Other sections of the boundary are defined by natural convection and radiation, if no significant shield gas flow influences these surfaces. The top side of the welded surface is typically defined by forced convection, due to shield gas flow from the weld torch nozzle. This area also emits radiation significantly, due to the heat source, which makes the workpiece reach the melting temperature.

The heat source in continuous welding is moving along a specified path where the process should accomplish a joining of workpiece members. There are several proposals in the literature for weld heat source models, and Goldak and Akhlaghi [**4**] provide

a comprehensive survey of different models and their applications. Here a model called Goldak's double ellipsoid [**4**] with a volumetric, Gaussian distribution-shaped heat flow density is used. It is a symmetric volume flux equation defined in a local coordinate system associated with the heat source. The heat source is $Q = \sum q_i$, where index $i = \mathrm{f}$, r denotes a separate distribution in the front f and rear r part of the heat source in the workpiece. The basic formula is

$$q_i = \frac{6\sqrt{3} f_i \eta V I}{\pi\sqrt{\pi} a b c_i} \exp\left(-3\frac{(x-x_1)^2}{a^2}\right) \times \exp\left(-3\frac{(y-y_1)^2}{b^2}\right) \exp\left(-3\frac{(z-z_1)^2}{c_i^2}\right) \quad (3)$$

where I is the weld current, η is the arc efficiency, and V is the arc voltage. The z-direction corresponds to the weld direction, and a, b, and c_i in the semi-axes of the ellipsoid define the extension in the x-, y-, and z-directions, respectively. To maintain continuity between the front and rear part, i.e. where $z = 0$ in the local coordinate system, the following condition must be fulfilled: $q_\mathrm{f}(t,x,y,0) = q_\mathrm{r}(t,x,y,0)$. This leads to a separate distribution of fractions of heat f_f and f_r in the front and rear part such that $f_\mathrm{f} + f_\mathrm{r} = 2$. The movement of the heat source is defined by $x_1(t)$,$y_1(t)$ $z_1(t)$, which denotes a moving coordinate in the surface of the workpiece.

Arc efficiency η is the fraction of weld arc heat energy that is transferred to the base metal and not lost to the environment. The total amount of heat generated in the arc is dissipated by radiation, convection, conduction, and evaporation from the arc column and to or from the base metal (see references [**16**, **19**, **20**]). Heat radiation causes both a heat transfer to the base metal and a heat loss to the ambient atmosphere, when it occurs in the arc. The heat radiation from the base metal only causes a heat loss to the ambient atmosphere. Heat convection in the arc occurs by means of the shielded gas flow including heat transfer to the base metal and a heat loss to the ambient atmosphere. The heat convection loss from the base metal is caused by natural and forced convection to the ambient atmosphere. Heat conduction occurs in the weld electrode and the base metal, and the heat conduction in the electrode contributes to a significant heat loss. Evaporation occurs in the weld pool, when the surface temperature exceeds the evaporation point. The total arc efficiency in GTAW can be estimated as [**16**]

$$\eta = 1 - \frac{q_\mathrm{electrode} + (1-n)q_\mathrm{arc} + m q_\mathrm{weld}}{VI} \quad (4)$$

where V and I are arc voltage and weld current, respectively. $q_\mathrm{electrode}$ (W) is the heat loss due to conduction in the weld electrode, q_arc is the heat radiated and convected from the arc column, and q_weld is the heat transferred to the base metal. The fraction of heat transferred from the arc to the base metal is n, and m is the fraction of radiation, convection, and evaporation losses in the base metal. Experimental studies estimate arc efficiency for GTAW in the range of 0.25 to 0.75 depending on the parameters and configuration used (see reference [**5**]).

3.2 Mechanical model

To predict the residual deformation, the classical theory of elasticity and thermo-plasticity is used in three dimensions [**5**, **21**]. Different mechanical boundary conditions are defined for different areas of the workpiece and fixture. The workpiece is deformable and the fixture is modelled as a rigid body. The stiff fastening at one side of the fixture is modelled by letting the boundaries be fixed in all Cartesian coordinates. Three different load cases were analysed. In the first case the variable end of the workpiece was loose and no force was applied. In the next two cases the variable end of the workpiece was clamped with medium and stiff clamping. These two cases were modelled with two rigid surfaces in contact with the workpiece and the frictional coefficient defining the Coulomb friction. Finally the applied force was loosened and the fixture surfaces were positioned 10 mm away from the plate after cooling. The Coulomb friction law is defined as [**18**]

$$\|f_\mathrm{t}\| < \mu f_\mathrm{n} \quad (5)$$

during the stick condition, and as

$$f_\mathrm{t} = -\mu f_\mathrm{n} \frac{v_\mathrm{r}}{\|v_\mathrm{r}\|} \quad (6)$$

during the slip condition, where μ is the frictional coefficient, f_t is the tangential friction force, f_n is the normal force, and v_r is the relative sliding velocity. To understand the importance of the friction, it was measured in the demonstrator and used as a known parameter in the simulations.

3.3 Material data

Thermo-physical properties of the base metal are the liquidus and solidification temperatures, density, thermal diffusivity, heat capacity, latent heat of fusion, and heat conductivity, which have been determined by experiments reported in reference [**12**]. An effective heat capacity with a latent heat component ΔL included is defined by

$$C_\mathrm{eff}(T) = \begin{cases} C(T), & T < T_\mathrm{sol} \\ C(T) + \frac{\Delta L}{T_\mathrm{liq} - T_\mathrm{sol}}, & T_\mathrm{sol} \leqslant T \leqslant T_\mathrm{liq} \\ C(T), & T > T_\mathrm{liq} \end{cases} \quad (7)$$

where $C(T)$ is heat capacity. The transition between solid and melted states is defined by the melting temperature T_{liq} and the solidification temperature T_{sol}. To imitate the increase in the heat conductivity due to the fluid flow that occurs in the weld pool, an increase in the heat conductivity k is introduced by multiplying k with a factor of ten when the temperature exceeds the melting temperature [**5**]. Mechanical properties are elastic modulus, Poisson's ratio, flow stress, and finally the thermo-mechanical property, thermal dilatation α. These data are provided in references [**23**] to [**26**]. Figure 6 shows temperature-dependent material properties and Fig. 7 shows the schematic relationship of temperature-dependent stress-strain data.

3.4 Finite element simulation

A 3D solid, quasi-coupled, thermally driven analysis has been performed, where 3120 elements of isoparametric distorted 3D brick elements with full integration were used (see e.g. reference [**27**]). The mesh density was highest along the weld path and, in order to resolve a more accurate solution, in the region close to the heat-affected zone. The general coarse mesh element size was 5 mm × 5 mm × 0.528 mm and the fine mesh element size was 2.5 mm × 2.5 mm × 0.528 mm; see Fig. 8 for the model. The parameters for the heat source model were $\eta = 0.75$, $a = 7$ mm, $b = 5$ mm, $c_f = 2.93$ mm, and $c_r = 5.87$ mm. These values were chosen as suggested by reference [**5**] and correspond to experimental geometrical data of the fusion zone. The model was implemented in MSC Marc Mentat 2005r3.

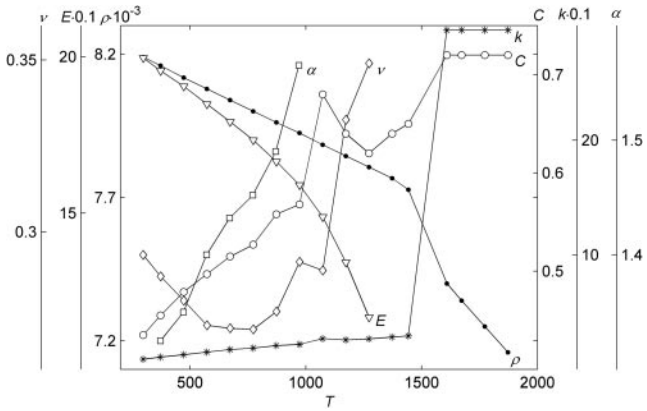

Fig. 6 Temperature-dependent physical properties of Inconel 718

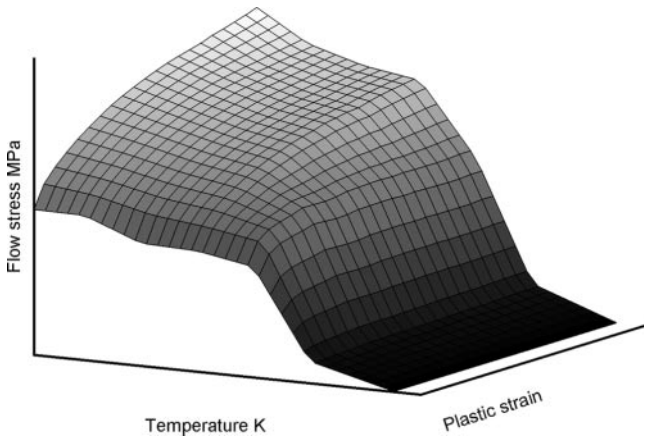

Fig. 7 Schematic temperature-dependent stress–strain relationship

4 RESULTS AND DISCUSSION

The friction test resulted in a frictional coefficient $\mu(0.95) = 0.2 \pm 0.012$, which was then used in the simulations. This number is a statistical average of four measurements at two levels of clamping force. Several other friction tests at different levels of clamping force were done. During these tests it was observed that the frictional coefficient increased slightly after every test performed, from approximately 0.2 up to approximately 0.36. The reason for this was that the sliding side between the contact surface of the plate and fixture become rougher for every test. When the sliding side was manually smoothened between the tests the frictional coefficient remained at 0.2. The interpretation of this is that the frictional coefficient is dependent on roughness due to wearing of the plate. The obtained value for the frictional coefficient is valid for a fresh plate. The Coulomb friction model works well in the demonstrator. Generally, when the normal force f_n becomes large, the Coulomb friction model may not show a good correlation with experimental observations. This is caused by the fact that the Coulomb model predicts that the frictional tangential force f_t increases to a level that can exceed the failure stress of the material. As this is not physically possible, a different friction calculation should be applied in these cases. There are several alternatives found in the literature on friction models [**18**].

The setup for the 3D scanning system results in a specified data noise level. This level is a sum of contributions from the noise in the CCD chip, optical distortion in the lenses, calibration routine of the system, the nature of the projected fringe pattern, etc. Since it is the specification of the geometrical tolerances for the workpiece that sets the demands on accuracy for the measurement equipment, it is

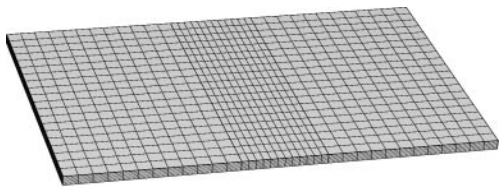

Fig. 8 Model and the mesh distribution of the plate

crucial to use a suitable measurement method. The experimental data collected arrived at a spatial accuracy of less than 0.025 mm, which was sufficient for detecting significant deformation. Results from these measurements were dense point clouds that were stitched together with the initial reference data. The stitching used a best-fit registration based on a minimizing a least square criterion. Local displacements as large as 0.5 mm were observed, indicating significant residual deformation. The reasons for using ATOS are that it is possible to do field measurement of total deformation in the workpiece and it is a comparatively robust, non-intrusive method suitable for environments such as those common in weld manufacturing. The system is also capable of producing sufficient data quality for the intended purposes.

The deformation measurements reveal the same typical distribution of deformations as the obtained simulation results. Deformation was not significant when the plate was still in the fixture, but after releasing, a difference was clearly observed between the different clamping forces. Table 2 provides simulated and measured values of spatial differences before and after the welding on plates that have been clamped with three levels of clamping forces. The values in Table 2 are the maximum deviations at the numbered points shown in Fig. 9. A comparison reveals an agreement between measurement and simulation that was expected; however, the simulated values are somewhat smaller. It is clear that the clamping force has a significant influence on the deformation: the larger the force, the larger the residual deformation. Figure 9 shows a grey-scale representation of deformation for a stiff (right) and loose clamped plate (left). The shape of the deformation is a uniform bending of the plate centred about the weld. This bending is very pronounced in the case of stiff clamping and not even noticeable in the case of loose clamping.

Another observation was that plates with mounted thermocouples exhibit larger deformation than plates without thermocouples. The distinction is significant. Figure 10 shows a grey-scale representation of deformation for the stiff case with (right) and without (left) thermocouples. The deviation in the plate normal between marks 1 and 2 for the plate without thermocouples compared with the deviation in the plate normal between marks 3 and 4 on the plate with thermocouples is 0.2 mm.

Temperature readings from the thermocouples are shown in Fig. 11. The weld time is shown as a black line and its duration is 42 s. The peak temperature is highest for thermocouples located closest to the weld path and the different peaks distributed in time correspond to the thermocouples located alongside the weld path. The agreement between this measured temperature history and the corresponding simulated result was very good and was used for validation of the simulation model.

Table 2 A summary of measured and simulated residual deformation

	Residual deformation (mm)	
Clamping case	Measured	Simulated
Loose clamping	0.30	0.20
Medium clamping	0.40	0.36
Stiff clamping	0.53	0.47

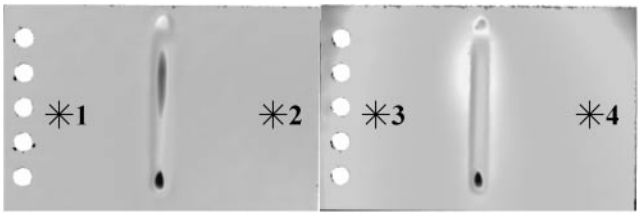

Fig. 9 Measured deviations: (left) measuring spots on loosely clamped plate; (right) corresponding data on stiff clamped plate

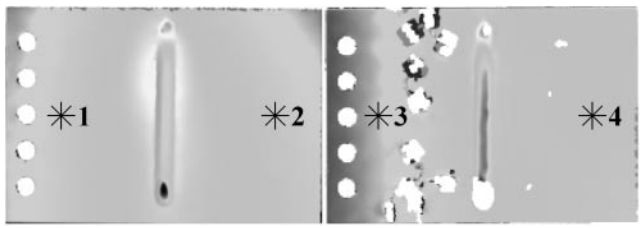

Fig. 10 Measured deviations: (left) measuring spots on plate without thermocouples; (right) corresponding data on plate with thermocouples

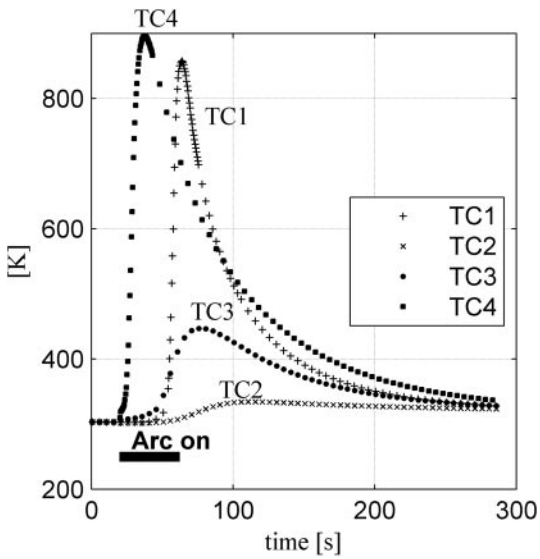

Fig. 11 Thermocouple responses during welding

5 CONCLUSIONS

Some lessons can be learned from the present work.

1. The measurement and simulation situations were not calibrated with the same reference system, which in the deformation respect implies that interpretation of the results must be undertaken with care. This is the reason for comparing measurements and simulations only at distinctive points. It is, however, encouraging that the correspondence is relatively good, and in continued work more emphasis should be placed on comparing exactly the same phenomena.
2. Optical 3D scanning could serve as a tool not only for model calibration and validation but also for quality control in weld manufacturing. It can detect residual deformation to a sufficient level of accuracy. It can also be said that by means of sufficiently accurate simulation models it is possible to predict the deformation, thus reducing the need for excessive measurements during weld manufacturing.
3. Use of thermocouples to acquire the temperature history during welding will also have an influence on the residual deformation. Any experimenter should be aware of this and take suitable precautions.
4. The fact that the clamping force is of great importance for the residual deformation calls for further research on control of fixture clamping forces.

All of the achieved knowledge above is of great importance for the high-tech aerospace industry, so that designers can more and more rely on their simulation models even for more complex components and non-uniform weld paths. The demonstrator was shown to be important for the future in that it can be used for validation of weld simulations for a number of other materials and other weld processes and for investigation of active fixture concepts comprising varying clamping forces.

ACKNOWLEDGEMENTS

This research work was supported in part by grants from the European Union within the Integrated Project AFFIX (IP NMP2-CT-2006-026670-AFFIX), which is gratefully acknowledged. The authors would like to thank Kjell Niklasson and Per Nylén, University West, for their valuable comments on the content and modelling aspects, and also Johan Molin, Volvo Aero Corporation, for his contribution in simulations.

REFERENCES

1 **Bolmsjö, G.** and **Olsson, M.** Sensors in robotic arc welding to support small series production. *Ind. Robot*, 2005, **32**(4), 341–345.
2 **Ericsson, M.** and **Nylen, P.** A look at the optimization of robot welding speed based on process modeling. *Welding J. (Miami, Fla)*, 2007, **86**(8), 238s–244s.
3 **Ericsson, M., Nylén, P., Berglund, D.,** and **Lin-Peng, R.** Three dimensional simulation of robot path, heat transfer and residual stresses of a welded part with complex geometry. *Int. J. Join. Mater.*, 2005, **17**(2), 42–51.
4 **Goldak, J. A.** and **Akhlaghi, M.** *Computational welding mechanics*, 2005 (Springer, New York, New York).
5 **Lindgren, L.-E.** *Computational welding mechanics: Thermomechanical and microstructructural simulations*, 2007 (CRC Press/Woodhead Publishing, Boca Raton, Florida/Cambridge, UK).
6 **Sikström, F.** and **Ericsson, M.** Integration of finite element analysis and computer aided robotics for advanced programming of robotized welding. In Proceedings of the 8th International Conference on Trends in Welding Research, Pine Mountain, Georgia, 2–5 June 2008 (ASM International, Ohio), pp. 454–460.
7 **Sikström, F., Ericsson, M., Christiansson, A.-K.,** and **Niklasson, K.** Tools for simulation based fixture design to reduce deformation in advanced fusion welding. In Proceedings of the 2nd International Conference on Intelligent Robotics and Applications (ICIRA2), Wuhan, China, 2008, vol. 5315 (Springer, Berlin/Heidelberg) pp. 398–407.
8 **Bag, S., De, A.,** and **DebRoy, T.** A genetic algorithm-assisted inverse convective heat transfer model for tailoring weld geometry. *Mater. Mfg Process.*, 2009, **24**(3), 384–397.
9 **Kumar, A.** and **DebRoy, T.** Heat transfer and fluid flow during gas-metal-arc fillet welding for various joint configurations and welding positions. *Metall. Mater. Trans. A: Phys. Metall. Mater. Sci.*, 2007, **38**(3), 506–519.
10 **Mishra, S., Lienert, T. J., Johnson, M. Q.,** and **DebRoy, T.** An experimental and theoretical study of gas tungsten arc welding of stainless steel plates with different sulfur concentrations. *Acta Mater.*, 2008, **56**(9), 2133–2146.
11 **Rai, R., Palmer, T. A., Elmer, J. W.,** and **Debroy, T.** Heat transfer and fluid flow during electron beam welding of 304L stainless steel alloy. *Welding J. (Miami, Fla)*, 2009, **88**(3), 54s–61s.
12 **Mills, K. C.** *Recommended values of thermo physical properties for selected commercial alloys*, 2002 (Woodhead Publishing Ltd, Cambridge, UK).
13 **Sikström, F., Ericsson, M., Nylén, P.,** and **Christiansson, A.-K.** 3D-scanning for weld distortion measuring. In Proceedings of the IEEE Instrumentation and Measurement Technology Conference, Sorrento, Italy, 24–27 April 2006, pp. 2132–2137.
14 **Bag, S.** and **De, A.** Development of a three-dimensional heat-transfer model for the gas tungsten arc welding process using the finite element method coupled with a genetic algorithm-based identification of uncertain

input parameters. *Metall. Mater. Trans. A: Phys. Metall. Mater. Sci.*, 2008, **39**(11), 2698–2710.
15 **Mughal, M., Fawad, H.,** and **Mufti, R.** Three-dimensional finite-element modelling of deformation in weld-based rapid prototyping. *Proc. IMechE, Part C: J. Mechanical Engineering Science*, 2006, **220**(6), 875–885. DOI: 10.1243/09544062JMES164.
16 **Nguyen, N. T.** *Thermal analysis of welds*, 2004 (WIT, Southampton, UK).
17 **Okui, N., Ketron, D., Bordelon, F., Hirata, Y.,** and **Clark, G.** A methodology for prediction of fusion zone shape. *Welding J. (Miami, Fla)*, 2007, **86**(2), 35s–43s.
18 **Hutchings, I. M.** *Tribology: Friction and wear of engineering materials*, 1992 (CRC Press, Boca Raton, Florida).
19 **Choi, M., Greif, R.,** and **Salcudean, M.** A study of the heat transfer during arc welding with applications to pure metals or alloys and low or high boiling temperature materials. *Numer. Heat Tran. A: Applic.*, 1987, **11**(4), 477–489.
20 **Zacharia, T., David, S.,** and **Vitek, J.** Effect of evaporation and temperature-dependent material properties on weld pool development. *Metall. Mater. Trans. B: Process Metall. Mater. Process.*, 1991, **22**(2), 233–241.
21 **Andersson, B. A. B.** Thermal stresses in a submerged-arc welded joint considering phase transformations. *J. Engng Mater. Technol.*, 1978, **100**(4), 356–362.
22 **Special Metals.** Inconel alloy 718, 2007, available from http://www.specialmetals.com (access date 23 February 2010).
23 **Lyphout, C., Nylén, P., Manescu, A.,** and **Pirling, T.** Residual stresses distribution through thick HVOF sprayed Inconel 718 coatings. *J. Thermal Spray Technol.*, 2008, **17**(5), 915–923.
24 **Sievert, R., Hamann, A.-H., Noack, D., Löwe, P., Singh, K. N.,** and **Künecke, G.** Simulation of thermal softening, damage and chip segmentation in a nickel super-alloy. In *Hochgeschwindigkeitspannen* (Eds H. K. Tönshoff and F. F. Hollmann), 2005, pp. 446–469 (Wiley-VCH, GmbH & Co. KGaA, Wienheim, Germany).
25 **Zhang, W. J., Reddy, B. V.,** and **Deevi, S. C.** Physical properties of TiAl-base alloys. *Scripta Mater.*, 2001, **45**(6), 645–651.
26 **Zienkiewicz, O. C., Taylor, R. L.,** and **Zhu, J. Z.** *The finite element method: Its basis and fundamentals*, 2005 (Elsevier Butterworth-Heinemann, Oxford, UK).

APPENDIX

Notation

C_{eff}, C	effective heat capacity, heat capacity (J/gK)
E	Young's modulus (GPa)
f_{n}	normal force (N)
f_{t}	tangential friction force (N)
h_{c}	convection heat transfer coefficient (W/m^{2}K)
I	current (A)
k	heat conductivity (W/mK)
Q, q_{XX}	rate of heat generated (W/m^3)
T	temperature (K)
v_{r}	relative sliding velocity (m/s)
V	voltage (V)
α	thermal expansion coefficient (1/K)
ε	emissivity
η	arc efficiency
μ	frictional coefficient
ν	Poisson's ratio
ρ	density (kg/m^3)
σ	Stefan-Boltzmann constant (W/m^{2}K^4)
σ_{P}	flow stress (MPa)